Aromaticity

An Open-Shell Coronoid with Hybrid Chichibabin–Schlenk Conjugation

Bibek Prajapati, Duy-Khoi Dang, Piotr J. Chmielewski, Marcin A. Majewski, Tadeusz Lis, Carlos J. Gómez-García, Paul M. Zimmerman,* and Marcin Stępień*

Dedicated to Professor Lechosław Latos-Grażyński on the occasion of his 70th birthday

Abstract: *A hexaradicaloid molecule with alternating Kekulé and non-Kekulé connectivities between adjacent spin centers was obtained by fusing two conjugation motifs in Chichibabin and Schlenk hydrocarbons into a coronoid structure. ^1H NMR, ESR, and SQUID experiments and computational analyses show that the system has a singlet ground state with a significant hexaradicaloid character ($\gamma_0 = 0.826$, $\gamma_1 = \gamma_2 = 0.773$). It has multiple thermally accessible high-spin states (up to the septet), with uniform energy gaps of ca. 1.0 kcal mol^{-1} between consecutive multiplicities. In line with its open-shell character, the coronoid has a small electronic band gap (ca. 0.8 eV) and undergoes two consecutive one-electron oxidations at low potentials, yielding cationic forms with extended near-infrared absorption. The hexaradicaloid, which combines open-shell and macrocyclic contributions to its π conjugation, is an example of a design strategy for multistate spin switches and redox-amphoteric NIR dyes.*

Introduction

Since their early discovery at the turn of the 20th century (**1**–**3**, Scheme 1),[1–3] open-shell organic molecules have attracted continued interest as a testing ground for theories of molecular bonding and electronic structure, and as an emerging class of organic materials.[4–14] Polyradicals derived from π-extended aromatics played an important role in these developments, as evidenced by their recent use as semiconductors,[15] near-infrared dyes,[16,17] cages,[18,19] switches,[20,21] and components for covalent self-assembly.[22–27] Embedding radicaloid centers in a circular π-conjugated array provides a way of studying the interplay between the

open-shell character and global (macrocyclic) aromaticity.[28,14] The interactions between spins are particularly enhanced in fully fused cyclic systems, that is, open-shell circulenes[29] and coronoids.[30–35] These systems are characterized by efficient p_z-orbital overlap and multiple conjugation pathways within their fused ring frameworks. They often combine unusual electronic structure characteristics with appreciable chemical stability. For instance, Wu's coronoid oligoradicals **4a,b** displayed unprecedented annulene-within-annulene (AWA) aromaticity that qualitatively depended on the size of the macrocycle.[31,36] The fully conjugated [4]chrysaorene **5**, reported concurrently by Wu and co-workers[32] and by our group,[33] displayed rich redox chemistry coupled with anion binding in the macrocyclic cavity.
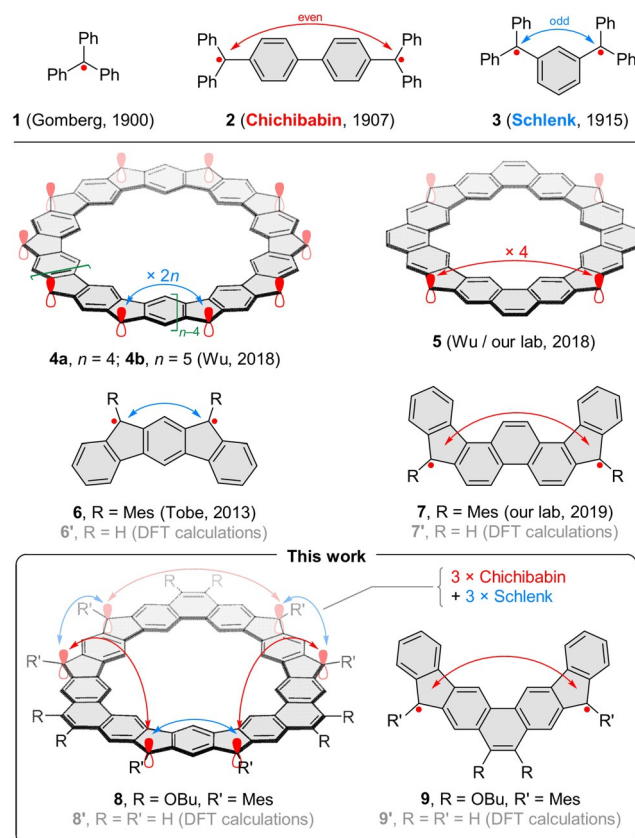
Scheme 1. Chichibabin and Schlenk conjugation in organic oligoradicaloids. Fully open-shell configurations shown for all oligoradicaloids. Substituents not shown for **4a,b** and **5**. Unpaired electrons are represented as red dots or p orbitals.

[*] B. Prajapati, Prof. P. J. Chmielewski, Dr. M. A. Majewski, Prof. T. Lis, Prof. M. Stępień
Wydział Chemii, Uniwersytet Wrocławski
ul. F. Joliot-Curie 14, 50-383 Wrocław (Poland)
E-mail: marcin.stepien@uwr.edu.pl

D.-K. Dang, Prof. P. M. Zimmerman
Department of Chemistry, University of Michigan
930 N. University Ave, Ann Arbor, MI 48109 (USA)
E-mail: paulzim@umich.edu

Prof. C. J. Gómez-García
Departamento de Química Inorgánica and
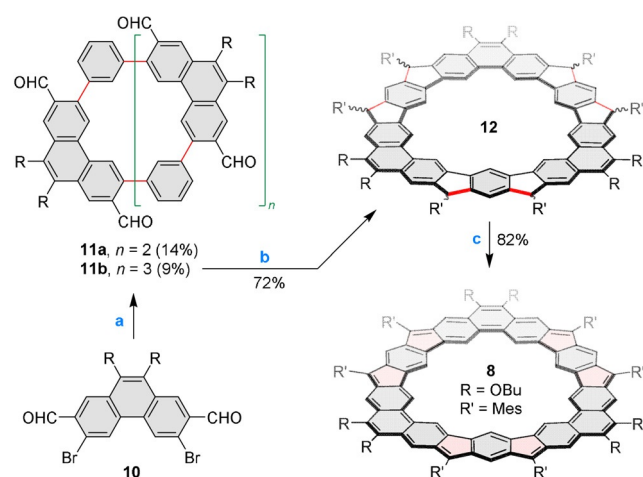Instituto de Ciencia Molecular, Universidad de Valencia
46980 Paterna (Spain)

Supporting information and the ORCID identification number(s) for the author(s) of this article can be found under:
https://doi.org/10.1002/anie.202109273.

In the open-shell coronoids studied so far, the interactions of adjacent spins were either fully equivalent, as in **4** and **5**, or topologically similar.[34,35] We reasoned that it might be possible to create systems that alternate between two interaction types to produce spin arrays with a more complex internal structure. With this goal in mind, we designed the coronoid system **8** that combines two classic conjugation types, those found, respectively in the Chichibabin[2,37] and Schlenk-Brauns[3,38] hydrocarbons (**2** and **3**, Scheme 1). The Chichibabin conjugation (Kekulé-type[10]) is characterized by an even-electron pathway between the interacting spins, and is thus fundamentally different from the Schlenk conjugation (non-Kekulé), which features an odd-electron path. This difference, which is reflected in the ground states of **2** (singlet[37]) and **3** (triplet[38]), creates an unusual structural dichotomy in the π-conjugated structure of **8**.

Hydrocarbons **2** and **3**, which contain only unfused benzene rings, have non-planar structures and are consequently relatively unstable. Robustness of such diradicaloids can be enhanced by indene fusion,[11,13] and steric protection, as illustrated by Tobe's indeno[2,1-*b*]fluorene **6**[39] and our own [1,2-*a*:2′,1′-*i*]phenanthrene **7**,[40] which feature, respectively the Schlenk- and Chichibabin-type conjugation embedded into a fused ring framework. In **8**, the radical centers are connected via alternating 2,7-phenanthrenylene and *meta*-phenylene subunits, which form a conjugation pattern that is simultaneously analogous to those found in **6** and in diindeno[2,1-*b*:1′,2′-*h*]phenanthrene **9**. The latter ring system is an isomer of **7**, and likewise features a Chichibabin-like conjugation pathway.
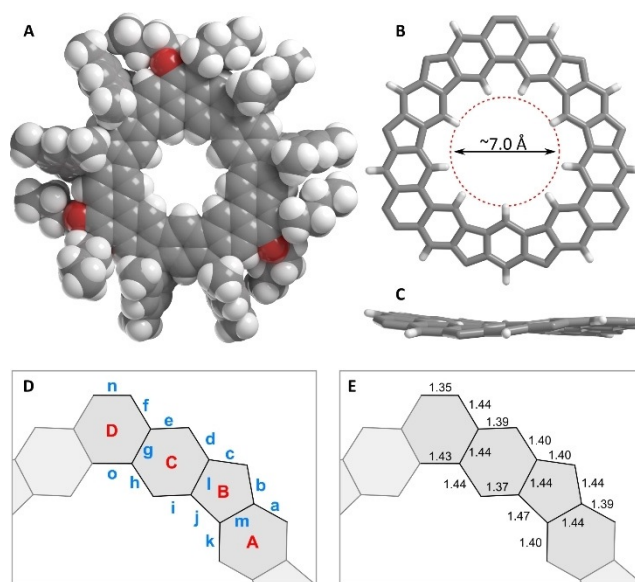
Results and Discussion

Coronoid **8** was obtained in a three-step synthesis from the phenanthrene building block **10** (Scheme 2).[41] First, the Suzuki condensation of **10** with 1,3-phenylenediboronic acid produced a mixture of products, from which the macrocycles 11a and 11b were isolated chromatographically. The desired larger macrocycle, **11b** was found to form a mixture of two conformations, which exchanged slowly on the ¹H NMR time scale. Interestingly, only one of these conformers is present in freshly synthesized **11b**, and the equilibrium between the two species is achieved after several days in chloroform solution. Compound **11b** was then subjected to sixfold Grignard addition followed by acid-catalyzed electrophilic cyclization, yielding the saturated precursor **12** as a mixture of stereoisomers. Among several methods used for dehydrogenation of **12**, the use of I$_2$/*t*-BuOK produced the cleanest results, furnishing the ultimate product **8** in 82% yield. The synthesis of the non-macrocyclic analogue **9** was carried out in a similar way, starting from **10** and phenylboronic acid (Supporting Information). Solutions of **8** and **9** can be handled in air, but they will degrade under ambient conditions after a couple of days.

When subjected to liquid–liquid diffusion in a [D$_8$]toluene/methanol solvent system, **8** formed two crystalline polymorphs, denoted A and B, which were characterized using XRD analysis (Figures 1 and S19,S20).[42] The molecules of **8** contain a rounded triangular cavity with an approximate diameter of 7 Å and are nearly, yet not completely planar. The intrinsic curvature of coronoid macrocycles depends on the fusion pattern of constituent rings. Briefly, the Gaussian curvature of the π system decreases with the increasing total number of rings and increases with the increasing number of five-membered rings in the coronoid molecule. Consequently, in reported coronoids the curvature ranges from positive (bowl-like),[43–45] through neutral,[32,33,46,47] to negative.[41,48] In both crystals, the coronoid ring system of **8** showed a slight saddle-shaped distortion from

Scheme 2. Synthesis of **8**. Reagents and conditions: a) 1,3-phenylene-diboronic acid (1.1 equiv), Pd(PPh$_3$)$_4$ (0.2 equiv), K$_2$CO$_3$ (10.0 equiv), dioxane, H$_2$O; b) 1. 2-MesMgBr (1 M solution in THF, 60.0 equiv), THF, 2. BF$_3$·Et$_2$O, DCM; c) 1. *t*-BuOK (2 M in 2-MeTHF, 18.0 equiv), THF, 2. I$_2$ (0.1 M in THF, 6.0 equiv).


Figure 1. Molecular structure of **8** determined in an X-ray diffraction analysis (polymorph B, solvent molecules and minor disordered positions are removed for clarity). A) Space-fill view; B and C) stick view with substituents removed for clarity. D) Labeling Scheme. E) Symmetry-averaged distances for polymorph B.

planarity, with a mean deviation from the average plane of 0.25 Å and 0.22 Å in polymorphs A and B, respectively. A simple geometrical analysis, assuming regular penta- and hexagonal rings, indicates that the molecule of **8** should indeed be negatively curved. However, gas-phase calculations predict a completely planar structure (see below), in which the excess curvature of **8** is transformed into distortions of valence angles. The out-of-plane distortion of this planar structure is associated with an ultra-low frequency vibrational mode (ca. 8 cm^{-1} for **8′**), and may be easily induced in the solid state by crystal packing forces. An analogous discrepancy between gas-phase and solid-state geometries was previously reported for septulene.[49]

The bond length pattern of **8** is similar in both polymorphs and shows approximate sixfold (D_{3h}-like) symmetry within the accuracy of crystal structure determinations (refinement esds of ca. 0.01 Å for C−C bond lengths). Symmetry-averaged interatomic distances (Figure 1E) disregard deviations from ideal symmetry caused, e.g., by crystal packing or admixtures of higher spin states (see below), but they nevertheless reveal statistically relevant trends in bond length patterns. The key C−C distances **b** and **c** in the 5-membered ring of **8** are 1.44 and 1.40 Å, respectively, i.e., they are comparable to the corresponding bond lengths in **7** (1.45 and 1.40 Å). Simultaneously, bond length **m** (1.44 Å in **8**) is relatively close to the analogous distance in **6** (1.45 Å). Importantly, the uniquely short bond length **n** (1.35 Å) and the markedly elongated distance **j** (1.47 Å) indicate significant localization of double- and single-bond character at these positions in the coronoid framework of **8**. Taken together, these features of compound **8** reveal an average bond length pattern intermediate between those of **6** and **7** (cf. Figure S8).

In common organic solvents at room temperature, **8** produced an extremely broadened ^{1}H NMR spectrum, with only the resonances of the butyl chains being clearly resolvable. The signals of the protons bound to the coronoid core became observable in dichlorofluoromethane-*d*, at temperatures below 200 K, indicating temperature-dependent paramagnetism of **8** and a singlet configuration in the ground state (Figure 2). The best resolution was achieved at 160 K, but the linewidths remained large (30–60 Hz), suggesting that paramagnetic forms might be significantly populated even at this temperature. Consequently, we were not able to record usable 2D correlation spectra. The ^{1}H NMR spectrum of **8** under these conditions contained two lines at 13.22 and 12.52 ppm with a 2:1 intensity ratio, assigned to the inner protons of the coronoid ring. These resonances were accompanied by three lines at 6.72, 6.22, and 5.14 ppm, with relative intensities of 4:2:1, assigned, respectively to the *m*-Mes and outer coronoid protons. Importantly, all resonances of the Mes substituents showed small upfield relocations relative to the corresponding shifts of the reference molecules **7** and **9** (Table S2). These chemical shift differences indicate the presence of a global paratropic current in the coronoid ring system of **8**, lending further support to the proposed assignment of signals. In comparison with [4]chrysaorene **5**,[33] the global paratropicity of **8** is however noticeably weaker.

SQUID measurements carried out for **8** and **9** revealed temperature-dependent magnetism consistent with a diamag-
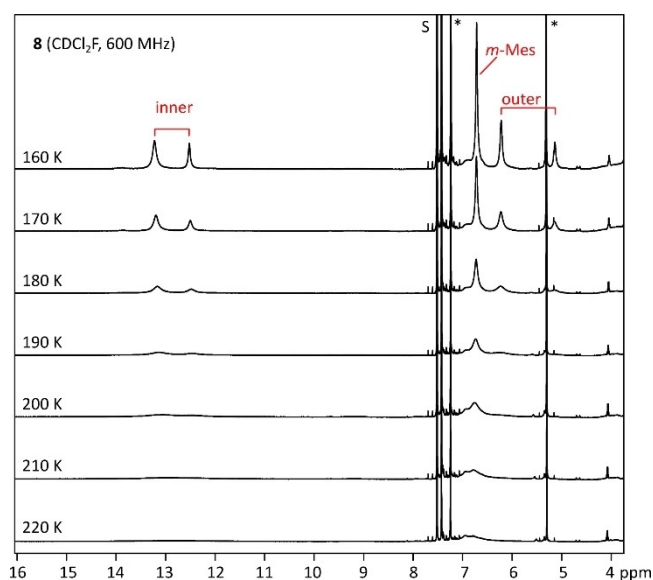
Figure 2. Variable-temperature ^{1}H NMR spectra recorded for **8** in dichlorofluoromethane-*d* (600 MHz, 160–220 K).

netic ground state of each system (Figure 3). Hexaradicaloid **8** showed a fully reversible $\chi_m T$ dependence in the 5–370 K temperature range, indicating appreciable thermal stability. The SQUID data could be precisely modeled with the Bleaney–Bowers equation by assuming three independent spin pairs and a fixed *g* value. This simplified model produced $J = -1.03$ kcal mol^{-1}, which can be interpreted as an apparent ΔE_{ST} gap of the system. A less accurate, yet similar *J* estimate of ca. -1.3 kcal mol^{-1} was obtained from a temperature-dependent ESR measurement (Figure S18). For the diradicaloid reference system **9** a somewhat larger value of $J = -1.20$ kcal mol^{-1} was obtained using SQUID, which is similar to the ΔE_{ST} estimates reported for the related diindenophenanthrene **7** (-1.2 to -1.3 kcal mol^{-1}).[40]

Compound **8** produced a relatively weak response in differential pulse voltammetry, apparently reflecting its limited chemical stability in solution. Two low-potential oxidation events were nevertheless observed at -0.16 and
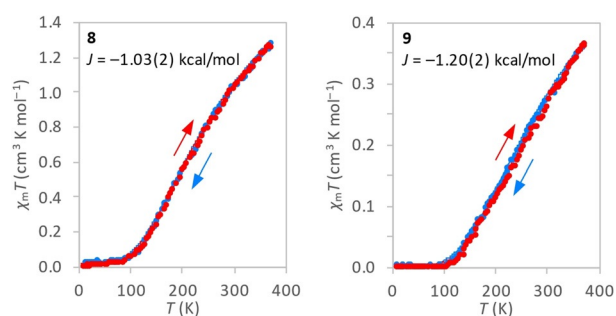

Figure 3. Thermal variation of the $\chi_m T$ product obtained for solid-state samples of compounds **8** (left) and **9** (right), using SQUID measurements (5 to 370 K temperature range). Red and blue data correspond, respectively to the heating and cooling run. The data were fitted with the Bleaney–Bowers model (fixed *g*, $S = \frac{1}{2}$ impurity content of 1.0% and 0.6% for **8** and **9**, respectively).

−0.06 V, followed by two additional oxidation peaks at 0.28 and 0.47 V (vs. Fc^+/Fc, Figure S6). **8** is thus slightly more difficult to oxidize than [4]chrysaorene **5** ($E_{ox1} = −0.18$ V, $E_{ox2} = −0.13$ V), in spite of its larger π-electron system. The first reduction event in **8** is however comparably more accessible (−0.99 V, vs. −1.26 V for **5**), yielding a small electrochemical band gap of only 0.83 V. In comparison, diindenophenanthrene **9**, which can be seen as a non-macrocyclic analogue of **8**, showed two reversible one-electron oxidations (0.10 and 0.52 V) and two reductions (−1.30 and −1.60 V, Figure S7), confirming the significant influence of coronoid conjugation on relative energies of charged states.

In solution, the neutral **8** has a green color, resulting from the presence of several distinct bands in the visible range of the spectrum (Figure 4, black trace). The spectrum contains additional weaker bands in the near-infrared (NIR) region, tailing at ca. 2000 nm. Such weak low-energy transitions are in line with the antiaromatic character of **8**, and resemble the features present in the spectrum of **5**. The apparent electronic band gap of **8** (ca. 0.75 eV corresponding to the shoulder at ca. 1650 nm) is however smaller than that of **5**, in agreement with the electrochemical results.

Coronoid **8** underwent a two-step oxidation when treated with oxidants such as $AgBF_4$, $AgPF_6$, $NOSbF_6$, or tris(4-bromophenyl)ammoniumyl hexachloroantimonate (BAHA, Figure 4). In all cases, the resulting absorption spectra were nearly identical and, since these oxidations could be induced using Ag^+ ($E^{\circ\prime} = 0.65$ V vs. Fc^+/Fc in CH_2Cl_2[50]),the two species were assigned as the mono- and dication **8**[+] and **8**[2+], respectively. Treatment of **8** with 1 equiv of a milder oxidant, diiodine, produced a near-quantitative conversion into the monocation **8**[+], whereas a much larger excess of I_2 was necessary to induce further conversion into **8**[2+]. This behavior closely resembled the I_2-induced oxidation of **5**,[33] reflecting the similarity of the E_{ox1} and E_{ox2} potentials of both species. The dication **8**[2+] could be converted back into the neutral **8** when the solution was treated with hydrazine hydrate (Figure S5). Addition of larger amounts of high-potential oxidants led to apparent decomposition of **8**.
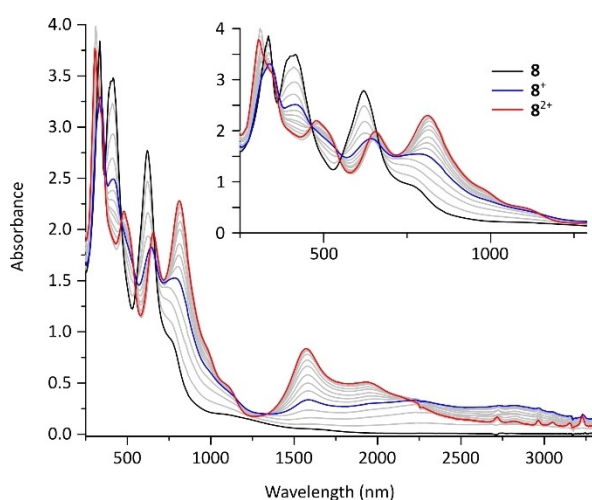
Figure 4. Stepwise oxidation of **8** (0.5 mM in $CDCl_3$) with BAHA (5 mM in MeCN-d_3). The blue and red traces correspond, respectively to the maximum concentration of **8**[+] and **8**[2+], respectively.

8[+] is brownish violet in solution and its absorption spectrum contains several broad bands in the NIR range, with maxima at 1585, 2191, and 2826 nm, and extending beyond 3300 nm (0.38 eV). The spectrum is qualitatively different from that of **5**[+] and indicates a smaller energy gap in **8**[+]. Significant NIR activity is also observed in the spectrum of the brownish blue **8**[2+], with absorption maxima at 1577 and 1934 nm. Titration of **8** with BAHA showed a significant increase of the doubly integrated ESR intensity up to ca. 0.5–0.7 equiv of the added oxidant (Figure S18). Further addition of BAHA resulted in a signal decrease to approximately the initial level. This behavior indicated that **8**[2+] might have a singlet ground state (similarly to **5**[2+]).

Gas-phase geometries of the four feasible spin states of substituent-free **8**′, i.e., singlet [1]**8**′, triplet [3]**8**′, quintet [5]**8**′, and septet [7]**8**′, were optimized at two different levels of theory: (a) dispersion-[51] and range-corrected[52] GD3BJ-CAM-B3LYP/6-31G(d,p), and (b) CASSCF(6,6)/cc-pVDZ[53,54] with the RICD approximation,[55,56] denoted, respectively CAM and CAS in subsequent discussion (Table 1). In all cases, the coronoid ring converged to a completely planar geometry. At both levels of theory, the singlet and septet optimizations yielded D_{3h}-symmetric geometries, while C_{2v}-symmetric structures were found for the triplet and quintet. The key features of the symmetry-averaged XRD structures of **8** were reproduced in the CAM and CAS geometries of [1]**8**′, notably (a) the relative similarity of bond lengths **b** and **c**, (b) the lengthening of the bond distance **j** and (c) the localization of a double bond at position **n**. In the septet geometries, the **c** bond was elongated, and the **b** bond was shortened relative to the corresponding distances in the singlets, but the bond length patterns were otherwise quite similar. Minor variations of C−C bond distances in[3]**8**′ and [5]**8**′ lead to reduction of point symmetry from D_{3h} to C_{2v}, apparently caused by the Jahn–Teller effect.

As a single-reference method, CAM is not suitable for quantitative analysis of open-shell species, although it correctly predicts that the different spin states of **8**′ should have similar energies, with a preference for the singlet configuration. RAS(6,6)-SF/cc-pVDZ[57,58] energies (E_{SF}) were calculated for the eight lowest electronic states at each of the optimized CAS geometries (Figures 5A and S2). At each geometry, the ground state was always found to be a singlet (S_0, $\langle S^2 \rangle = 0$), followed consecutively by three triplets (T_1

Table 1: Computational details for the adiabatic spin states of **8**′.

State	[1]**8**′-S_0	[3]**8**′-T_1	[5]**8**′-Qn_1	[7]**8**′-Sp_1
Point symmetry[a]	D_{3h}	C_{2v}	C_{2v}	D_{3h}
ΔE_{CAM} [kcal mol^{-1}][b]	0.00	1.64	0.79	0.10
ΔE_{SF} [eV][c,d]	0.000	0.043	0.084	0.129
ΔE_{SF} [kcal mol^{-1}][c,d]	0.00	0.99	1.94	2.97
n_U[c,d,e]	4.746	5.229	5.633	6.000

[a] Point symmetries of optimized geometries. [b] GD3BJ-CAM-B3LYP/6-31G(d,p) electronic energies. [c] RAS(6,6)-SF/cc-pVDZ// CASSCF(6,6)/cc-pVDZ. [d] Lowest-energy state with a given multiplicity at the corresponding optimized CAS geometry. [e] $n_U = \sum_i(1 - |1 - n_i|)$, where n_i is the NO occupation number obtained from SF calculations and i runs over the six frontier orbitals.

Angew. Chem. Int. Ed. **2021**, *60*, 22496–22504

© 2021 Wiley-VCH GmbH

www.angewandte.org **22499**
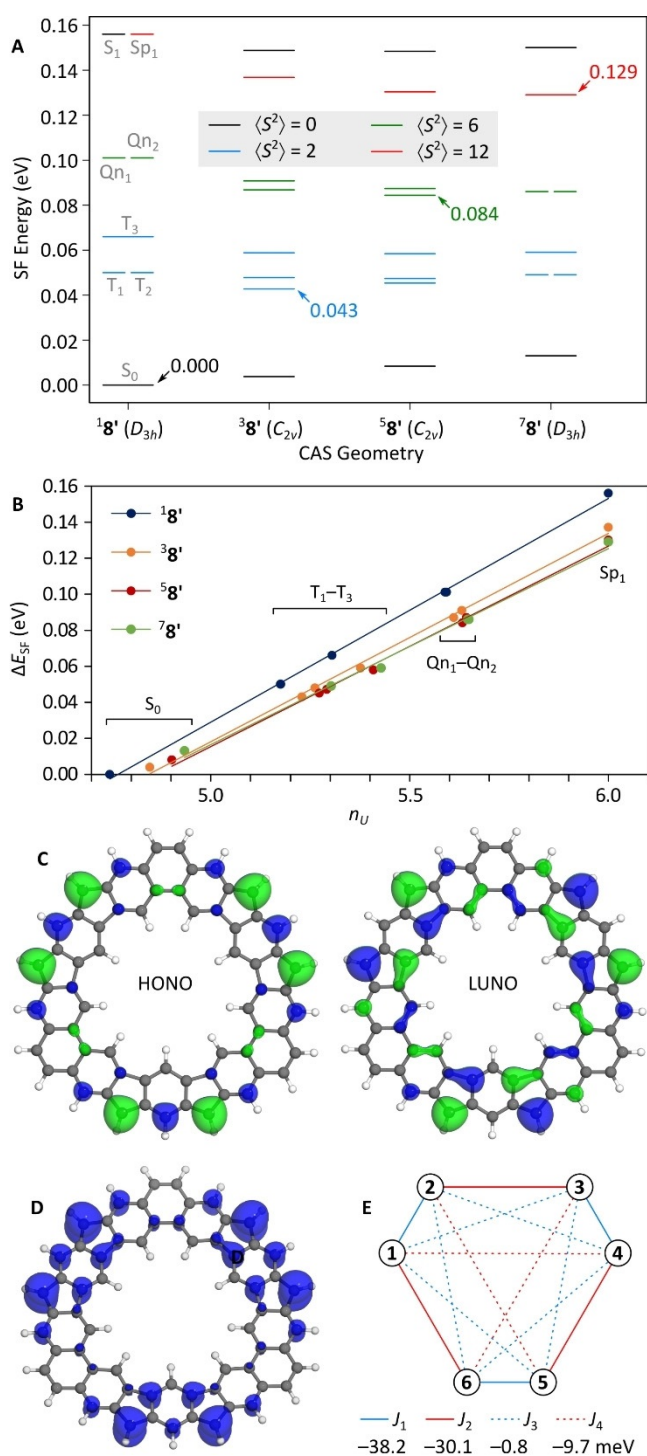
Figure 5. A) SF energies and spins of the first eight states of **8′** calculated at optimized CAS geometries of different spin states of **8′**. The lowest-energy state for a given spin multiplicity is indicated with an arrow. The singlet geometry ¹**8′** has a 6-fold degeneracy at 0.156 eV consisting of three singlets and two triplets and one septet state. B) Relationship between ΔE_{SF} and the number of unpaired electrons n_U derived from natural orbital occupation numbers. C) Frontier natural orbitals for the ¹**8′**-S₀ state (0.02 a.u. isosurface). D) SF odd-electron density for ¹**8′** (0.002 a.u. isosurface). E) Definition of coupling constants used in an approximate spin Hamiltonian (see text). *J* values are given for the ¹**8′**-S₀ state.

through T₃, ↑S^2⟩ = 2), two quintets (Qn₁ and Qn₂, ↑S^2⟩ = 6), one septet (Sp₁, ↑S^2⟩ = 12) and one singlet state (S₁). For the D_{3h}-symmetric structures (¹**8′** and ⁷**8′**), the two lowest-energy triplet excitations T₁ and T₂ were degenerate, and analogous degeneracies were found for the Qn₁ and Qn₂ quintets. These degeneracies are indicative of spin frustration,[59] and account for the Jahn–Teller distortion found for ³**8′** and ⁵**8′** at the CAM and CAS levels.

For each multiplicity, the lowest SF energy was identified at the corresponding CAS geometry (S₀ at ¹**8′**, T₁ at ³**8′**, etc., Table 1), confirming the consistency of the SF and CAS approaches. Relative SF energies of the adiabatic states ¹**8′**, ³**8′**, ⁵**8′**, and ⁷**8′** are thus 0.00, 0.99, 1.94, 2.97 kcal mol⁻¹, that is, the energy rises by a nearly constant value of ca. 1 kcal mol⁻¹ per each increase in multiplicity. This value is smaller than the SF-based estimates of ΔE_{ST} obtained for **5′** (−6.60 kcal mol⁻¹)[33] and **7′** (R = H, −1.29 kcal mol⁻¹).[40] An interaction model constructed on the basis of SF excitation energies suggests that couplings between all spin pairs in **8′** are effectively antiferromagnetic in character (Figure 5E, see the Supporting Information for a detailed discussion).

Natural orbitals (NOs) and the corresponding occupation numbers (NOONs)[60] obtained from the SF densities provided additional insight into the ground and excited states of **8′** (Figures S11–S17). For all of these states, amplitudes of the frontier NOs may be approximated as linear combinations of singly occupied molecular orbitals corresponding to the three embedded *m*-xylylene[10] fragments. This feature, which is most evident in the HONO and LUNO of ¹**8′**-S₀ (Figure 5C), suggest a Schlenk-like behavior of the unpaired electrons in the system. A similar picture is provided by the SF odd-electron density determined for ¹**8′**-S₀ (Figure 5D). The NOONs of ¹**8′**-S₀ yielded high polyradicaloid indices $\gamma_0 = 0.826$ and $\gamma_1 = \gamma_2 = 0.773$ (Figure S1), confirming the open-shell character of the singlet state. In comparison, indices based on the CAM density were $\gamma_0 = 0.984$ and $\gamma_1 = \gamma_2 = 0.559$. Similarly, the number of unpaired electrons n_U,[61] derived from SF NOONs is very high for ¹**8′**-S₀ ($n_U = 4.746$, Table 1). The n_U values of excited states increase with their increasing multiplicity and are larger than the total spin ($n_U > 2S$), except for the septet (Sp₁) configurations, for which $n_U = 2S = 6$. In particular, the n_U index differentiates excitations with the same S; for instance, n_U is 5.18 for ¹**8′**-T₁ and ¹**8′**-T₂, and 5.30 for ¹**8′**-T₃. Interestingly, for each CAS geometry, there is an excellent linear correlation between the SF energy, ΔE_{SF}, and the n_U index (Figure 5B). The slope of this dependence (0.124 eV/electron or 2.86 kcal mol⁻¹/electron for ¹**8′**) provides an alternative measure of electron pairing energy that considers the multiconfigurational nature of all states.

Anisotropy of the induced current density (ACID)[62] reveled distinct differences between π electron delocalization in **8′** and the non-macrocyclic references **9′** and **7′** (Figure 6). **9′** contains three major diatropic (clockwise) currents: two in the outer benzene rings, and one encompassing the central phenanthrene subunit. Each of these currents is somewhat perturbed in comparison with the corresponding parent arene, however, there is no significant circulation in the five-membered rings of **9′**, although the ACID density is

22500   www.angewandte.org

© 2021 Wiley-VCH GmbH

Angew. Chem. Int. Ed. **2021**, *60*, 22496–22504
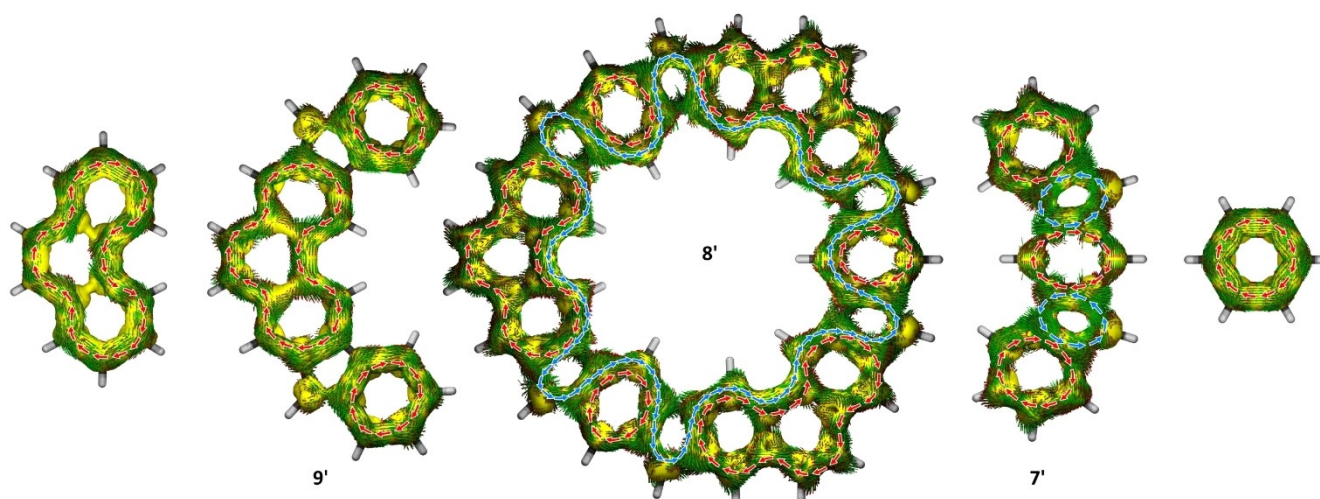
Figure 6. Anisotropy of induced current density (ACID) plots for π electrons of phenanthrene, [1]6′, [1]7′, [1]8′, and benzene (CSGT/CAM, 0.03 a.u. isovalues). Major clockwise and anticlockwise currents are indicated, respectively with red and blue arrows.

significant at the methine bridges. In contrast, benzenoid delocalization is very strongly perturbed in **7′**, which shows strong paratropic (anticlockwise) circulations in the five-membered rings. An intermediate case of delocalization is observed in **8′**, sharing features found in **7′** and **9′**. Interestingly, the superposition of local currents in **8′** produces a macrocyclic delocalization pathway consisting of 45 atoms. The paratropic nature of this global current is consistent with the experimental ^{1}H NMR signature of **8**.

The nucleus-independent chemical shift (NICS)[63] mapped 1 Å above the molecular plane of **8′** revealed spin state-dependent changes of local and global magnetism of the coronoid ring system (Figure 7). In the singlet state [1]**8′**, local ring currents in the six-membered rings A, C, and D are significantly weakened in comparison with isolated benzene and phenanthrene. The paratropicity of the five-membered rings increases in the order **9′** < [1]**8′** < **6′**, and the local magnetism of the coronoid may be seen as an average of the features observed in the non-macrocyclic references. The interior of the coronoid is moderately shielded in in line with the experimentally observed global paratropicity of **8**. Calculated shifts of the inner protons of **8′** (8.71 and 8.32 ppm) are however much smaller than the experimental values (13.22 and 12.52 ppm). Thus, the CAM level of theory significantly underestimates the global ring current in **8′**, likely because of the highly multiconfigurational character of the singlet state. In the septet state, [7]**8′**, the local aromaticity of phenanthrene subunits is partly recovered (rings C and D), whereas the diatropicity of benzene ring A is even weaker than in the singlet state. The septet can thus be described as a union of three Schlenk diradicals (each in the triplet state), which are relatively weaky coupled to the intervening phenanthrene subunits. In the intermediate spin states, [3]**8′** and [5]**8′**, a gradual transition is observed between the weak local diatropicity of [1]**8′** and the phenanthrene-like character of [7]**8′**. The changes are however not uniform in [3]**8′** and [5]**8′**, reflecting the local differences in π conjugation caused by Jahn–Teller distortions.
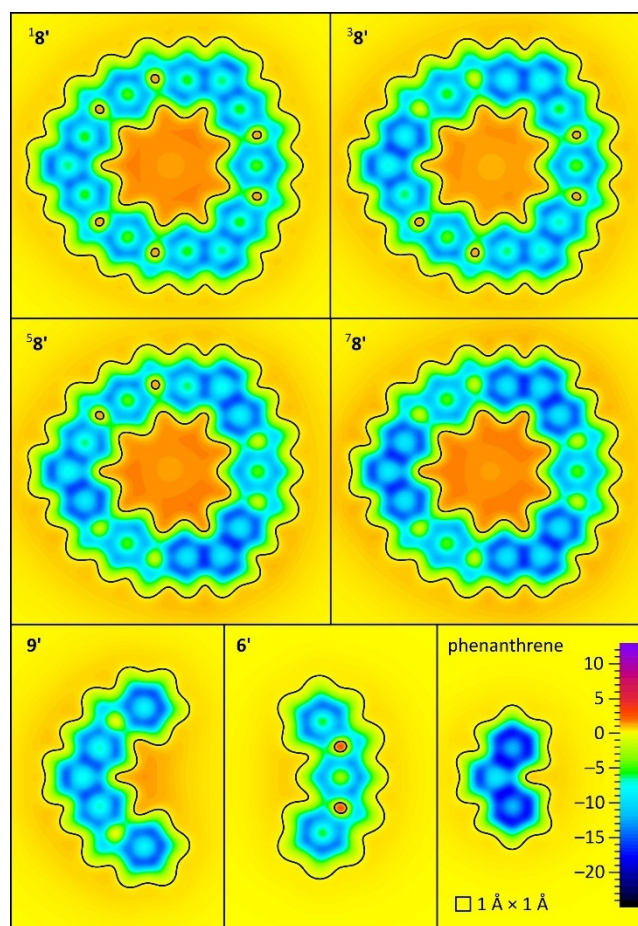
Figure 7. NICS(1) maps for the four spin states of **8′** and reference polycyclic systems evaluated at the GIAO/CAM level of theory.

Additional insight into the structure of **8** can be gained from the conventional valence bond analysis of its singlet state (Scheme 3). Configuration **8′**-I maximizes the number of unpaired electrons, while producing the highest number of
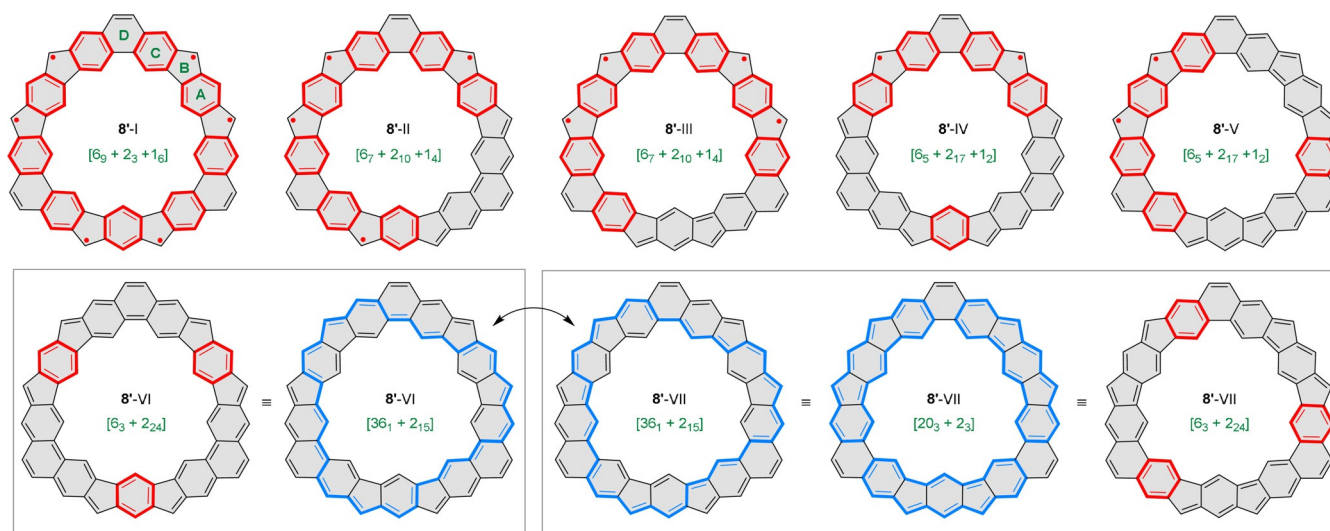
Scheme 3. Selected canonical structures of **8′**. Formally aromatic and antiaromatic circuits are shown in red and blue, respectively. π-Electron partitioning (green labels) corresponds to the highlighted circuits.

Clar sextets, which occupy all available rings **A** and **C**. This partitioning may be denoted $[6_9 + 2_3 + 1_6]$, where the consecutive terms correspond, respectively to the nine Clar sextets (6_9), three double bonds not involved in cyclic circuits (2_3), and 6 radical centers (1_6; the total number of π electrons in **8′** is 66). A tetraradicaloid structure is now built by pairing two adjacent radical centers along one of the three "phenanthrene edges," which thus becomes completely quinoidal. The resulting configuration **8′**-II contains 7 sextets and can be described as $[6_7 + 2_{10} + 1_4]$. It is possible to build other distinct tetraradicaloid configurations with the same electron partitioning but a different placement of radical centers (e.g. **8′**-III), as well as configurations with fewer Clar sextets. Diradicaloid configurations can be built similarly (e.g. **8′**-IV and **8′**-V), and they can contain up to five sextets, reflected in the $[6_5 + 2_{17} + 1_2]$ partitioning.

The high numbers of Clar sextets in **8′**-I-V are responsible for the relatively significant contributions of these structures to the singlet state and the stability of high-spin states of **8**. Complete pairing of all radical sites along the phenanthrene edges of **8′** produces the fully closed-shell configuration **8′**-VI, in which three Clar sextets in rings **A** yield a $[6_3 + 2_{24}]$ partitioning. Scheme 3 additionally shows one of several $[36_1 + 2_{15}]$ divisions that are possible for structure **8′**-VI. The macrocyclic conjugation pathway defined by the latter partitioning corresponds to the Kekulé pair consisting of **8′**-VI and **8′**-VII. With a 4n-electron count, this pathway should correspond to Hückel antiaromaticity, and its presence may explain the paratropic ring current in **8** observed by ^{1}H NMR at low temperatures. Double bonds in **8′**-VII can also be partitioned into three 20-electron dibenzoindacene circuits ($[20_3 + 2_3]$), each corresponding to the closed-shell configuration of indeno[2,1-*b*]fluorene **7**. Finally, the $[6_3 + 2_{24}]$ partitioning, with three Clar sextets located in rings **C**, is also possible for **8′**-VII.

Coronoid π systems can be partitioned into two concentric annulene-like circuits, each of which normally contains an even number of electrons (e.g. $[30 + 18]$ for kekulene, $[40 + 30]$ for **4b**, and $[36 + 24]$ for **5**). The fusion pattern and threefold symmetry of **8′** result in an odd-electron $[39 + 27]$ partitioning. The presence of two odd-electron circuits, previously reported for septulene ($[35 + 21]$),[49] indicates that the outer and inner circuits in **8′** cannot be fully decoupled in a closed-shell configuration, that is, the AWA aromaticity is ruled out for topological reasons.

Conclusion

This work describes the first example of an open-shell coronoid molecule, in which Kekulé and non-Kekulé conjugation pathways are juxtaposed in a cyclic oligoradical array. Locally, this system shares features of the Schlenk and Chichibabin hydrocarbons, to which it is structurally related, but it also displays global characteristics resulting from macrocyclic conjugation. In particular, it has a singlet ground state with a highly multiconfigurational character, but the three high-spin states, triplet, quintet, and septet, have low energies and are significantly populated at room temperature. The system is further notable for its macrocyclic paratropicity, spanning a 36-electron conjugation circuit, remarkably low redox potentials, and small energy gaps in all of its three stable oxidation levels. The present work shows that coronoid motifs are suitable platforms for building stable oligoradicals with high spin densities, and that the ring fusion topology has a strong influence on collective properties of the embedded spin centers. We are currently exploring other designs of open-shell coronoids, which may shed more light on the complex relationship between their structure and oligoradicaloid characters.

© 2021 Wiley-VCH GmbH

Conflict of Interest

The authors declare no conflict of interest.

Keywords: aromaticity · coronoids · molecular magnetism · radicaloids · spectroscopy

[1] M. Gomberg, *Ber. Dtsch. Chem. Ges.* **1900**, *33*, 3150–3163.

[2] A. E. Tschitschibabin, *Ber. Dtsch. Chem. Ges.* **1907**, *40*, 1810–1819.

[3] W. Schlenk, M. Brauns, *Ber. Dtsch. Chem. Ges.* **1915**, *48*, 661–669.

[4] D. A. Dougherty, *Acc. Chem. Res.* **1991**, *24*, 88–94.

[5] A. Rajca, *Chem. Rev.* **1994**, *94*, 871–893.

[6] M. Abe, *Chem. Rev.* **2013**, *113*, 7011–7088.

[7] Z. Sun, Z. Zeng, J. Wu, *Acc. Chem. Res.* **2014**, *47*, 2582–2591.

[8] Z. Zeng, X. Shi, C. Chi, J. T. L. Navarrete, J. Casado, J. Wu, *Chem. Soc. Rev.* **2015**, *44*, 6578–6596.

[9] T. Kubo, *Chem. Rec.* **2015**, *15*, 218–232.

[10] N. M. Gallagher, A. Olankitwanit, A. Rajca, *J. Org. Chem.* **2015**, *80*, 1291–1298.

[11] C. K. Frederickson, B. D. Rose, M. M. Haley, *Acc. Chem. Res.* **2017**, *50*, 977–987.

[12] J. Casado, *Top. Curr. Chem.* **2017**, *375*, 73.

[13] Y. Tobe, *Top. Curr. Chem.* **2018**, *376*, 12.

[14] C. Liu, Y. Ni, X. Lu, G. Li, J. Wu, *Acc. Chem. Res.* **2019**, *52*, 2309—2321.

[15] G. E. Rudebusch, J. L. Zafra, K. Jorner, K. Fukuda, J. L. Marshall, I. Arrechea-Marcos, G. L. Espejo, R. Ponce Ortiz, C. J. Gómez-García, L. N. Zakharov, M. Nakano, H. Ottosson, J. Casado, M. M. Haley, *Nat. Chem.* **2016**, *8*, 753–759.

[16] Y. Ni, S. Lee, M. Son, N. Aratani, M. Ishida, A. Samanta, H. Yamada, Y.-T. Chang, H. Furuta, D. Kim, J. Wu, *Angew. Chem. Int. Ed.* **2016**, *55*, 2815–2819; *Angew. Chem.* **2016**, *128*, 2865–2869.

[17] K. Okino, D. Sakamaki, S. Seki, *ACS Mater. Lett.* **2019**, *1*, 25–29.

[18] X. Gu, T. Y. Gopalakrishna, H. Phan, Y. Ni, T. S. Herng, J. Ding, J. Wu, *Angew. Chem. Int. Ed.* **2017**, *56*, 15383–15387; *Angew. Chem.* **2017**, *129*, 15585–15589.

[19] Y. Ni, T. Y. Gopalakrishna, H. Phan, T. Kim, T. S. Herng, Y. Han, T. Tao, J. Ding, D. Kim, J. Wu, *Nat. Chem.* **2020**, *12*, 242–248.

[20] P. Ravat, T. Šolomek, D. Häussinger, O. Blacque, M. Juríček, *J. Am. Chem. Soc.* **2018**, *140*, 10839–10847.

[21] D. Shimizu, Y. Ide, T. Ikeue, A. Osuka, *Angew. Chem. Int. Ed.* **2019**, *58*, 5023–5027; *Angew. Chem.* **2019**, *131*, 5077–5081.

[22] D. Beaudoin, O. Levasseur-Grenon, T. Maris, J. D. Wuest, *Angew. Chem. Int. Ed.* **2016**, *55*, 894–898; *Angew. Chem.* **2016**, *128*, 906–910.

[23] K. Oda, S. Hiroto, H. Shinokubo, *J. Mater. Chem. C* **2017**, *5*, 5310–5315.

[24] H. Yokoi, S. Hiroto, H. Shinokubo, *J. Am. Chem. Soc.* **2018**, *140*, 4649–4655.

[25] L. Yuan, Y. Han, T. Tao, H. Phan, C. Chi, *Angew. Chem. Int. Ed.* **2018**, *57*, 9023–9027; *Angew. Chem.* **2018**, *130*, 9161–9165.

[26] L. Moshniaha, M. Żyła-Karwowska, P. J. Chmielewski, T. Lis, J. Cybińska, E. Gońka, J. Oschwald, T. Drewello, S. M. Rivero, J. Casado, M. Stępień, *J. Am. Chem. Soc.* **2020**, *142*, 3626–3635.

[27] K. Sahara, M. Abe, H. Zipse, T. Kubo, *J. Am. Chem. Soc.* **2020**, *142*, 5408–5418.

[28] H. Miyoshi, S. Nobusue, A. Shimizu, Y. Tobe, *Chem. Soc. Rev.* **2015**, *44*, 6560–6577.

[29] S. Nobusue, H. Miyoshi, A. Shimizu, I. Hisaki, K. Fukuda, M. Nakano, Y. Tobe, *Angew. Chem. Int. Ed.* **2015**, *54*, 2090–2094; *Angew. Chem.* **2015**, *127*, 2118–2122.

[30] S. Das, T. S. Herng, J. L. Zafra, P. M. Burrezo, M. Kitano, M. Ishida, T. Y. Gopalakrishna, P. Hu, A. Osuka, J. Casado, J. Ding, D. Casanova, J. Wu, *J. Am. Chem. Soc.* **2016**, *138*, 7782–7790.

[31] C. Liu, M. E. Sandoval-Salinas, Y. Hong, T. Y. Gopalakrishna, H. Phan, N. Aratani, T. S. Herng, J. Ding, H. Yamada, D. Kim, D. Casanova, J. Wu, *Chem* **2018**, *4*, 1586–1595.

[32] X. Lu, T. Y. Gopalakrishna, H. Phan, T. S. Herng, Q. Jiang, C. Liu, G. Li, J. Ding, J. Wu, *Angew. Chem. Int. Ed.* **2018**, *57*, 13052–13056; *Angew. Chem.* **2018**, *130*, 13236–13240.

[33] H. Gregolińska, M. Majewski, P. J. Chmielewski, J. Gregoliński, A. Chien, J. Zhou, Y.-L. Wu, Y. J. Bae, M. R. Wasielewski, P. M. Zimmerman, M. Stępień, *J. Am. Chem. Soc.* **2018**, *140*, 14474–14480.

[34] X. Lu, T. Y. Gopalakrishna, Y. Han, Y. Ni, Y. Zou, J. Wu, *J. Am. Chem. Soc.* **2019**, *141*, 5934–5941.

[35] X. Lu, D. An, Y. Han, Y. Zou, Y. Qiao, N. Zhang, D. Chang, J. Wu, Y. Liu, *Chem. Sci.* **2021**, *12*, 3952–3957.

[36] M. Stępień, *Chem* **2018**, *4*, 1481–1483.

[37] L. K. Montgomery, J. C. Huffman, E. A. Jurczak, M. P. Grendze, *J. Am. Chem. Soc.* **1986**, *108*, 6004–6011.

[38] G. Kothe, K.-H. Denkel, W. Sümmermann, *Angew. Chem. Int. Ed. Engl.* **1970**, *9*, 906–907; *Angew. Chem.* **1970**, *82*, 935–937.

[39] A. Shimizu, R. Kishi, M. Nakano, D. Shiomi, K. Sato, T. Takui, I. Hisaki, M. Miyata, Y. Tobe, *Angew. Chem. Int. Ed.* **2013**, *52*, 6076–6079; *Angew. Chem.* **2013**, *125*, 6192–6195.

[40] M. A. Majewski, P. J. Chmielewski, A. Chien, Y. Hong, T. Lis, M. Witwicki, D. Kim, P. M. Zimmerman, M. Stępień, *Chem. Sci.* **2019**, *10*, 3413–3420.

[41] M. A. Majewski, Y. Hong, T. Lis, J. Gregoliński, P. J. Chmielewski, J. Cybińska, D. Kim, M. Stępień, *Angew. Chem. Int. Ed.* **2016**, *55*, 14072–14076; *Angew. Chem.* **2016**, *128*, 14278–14282.

[42] Deposition Numbers 2087057 (for polymorph A), and 2087056 (for polymorph B) contain the supplementary crystallographic data for this paper. These data are provided free of charge by the joint Cambridge Crystallographic Data Centre and Fachinformationszentrum Karlsruhe Access Structures service www.ccdc.cam.ac.uk/structures.

[43] D. Myśliwiec, M. Stępień, *Angew. Chem. Int. Ed.* **2013**, *52*, 1713–1717; *Angew. Chem.* **2013**, *125*, 1757–1761.

[44] M. A. Majewski, T. Lis, J. Cybińska, M. Stępień, *Chem. Commun.* **2015**, *51*, 15094–15097.

[45] H. Hou, X.-J. Zhao, C. Tang, Y.-Y. Ju, Z.-Y. Deng, X.-R. Wang, L.-B. Feng, D.-H. Lin, X. Hou, A. Narita, K. Müllen, Y.-Z. Tan, *Nat. Commun.* **2020**, *11*, 3976.

[46] F. Diederich, H. A. Staab, *Angew. Chem. Int. Ed. Engl.* **1978**, *17*, 372–374; *Angew. Chem.* **1978**, *90*, 383–385.

[47] U. Beser, M. Kastler, A. Maghsoumi, M. Wagner, C. Castiglioni, M. Tommasini, A. Narita, X. Feng, K. Müllen, *J. Am. Chem. Soc.* **2016**, *138*, 4322–4325.

[48] Y. Yang, M. Chu, Q. Miao, *Org. Lett.* **2018**, *20*, 4259–4262.

[49] B. Kumar, R. L. Viboh, M. C. Bonifacio, W. B. Thompson, J. C. Buttrick, B. C. Westlake, M.-S. Kim, R. W. Zoellner, S. A. Varganov, P. Mörschel, J. Teteruk, M. U. Schmidt, B. T. King, *Angew. Chem. Int. Ed.* **2012**, *51*, 12795–12800; *Angew. Chem.* **2012**, *124*, 12967–12972.

[50] N. G. Connelly, W. E. Geiger, *Chem. Rev.* **1996**, *96*, 877–910.

[51] S. Grimme, S. Ehrlich, L. Goerigk, *J. Comput. Chem.* **2011**, *32*, 1456–1465.

[52] T. Yanai, D. P. Tew, N. C. Handy, *Chem. Phys. Lett.* **2004**, *393*, 51–57.

[53] B. O. Roos, *Int. J. Quantum Chem.* **1980**, *18*, 175–189.

[54] B. O. Roos, P. R. Taylor, P. E. M. Sigbahn, *Chem. Phys.* **1980**, *48*, 157–173.

[55] F. Aquilante, T. B. Pedersen, R. Lindh, *J. Chem. Phys.* **2007**, *126*, 194106.

[56] J. Boström, F. Aquilante, T. B. Pedersen, R. Lindh, *J. Chem. Theory Comput.* **2009**, *5*, 1545–1553.

[57] P. M. Zimmerman, F. Bell, M. Goldey, A. T. Bell, M. Head-Gordon, *J. Chem. Phys.* **2012**, *137*, 164110.

[58] F. Bell, P. M. Zimmerman, D. Casanova, M. Goldey, M. Head-Gordon, *Phys. Chem. Chem. Phys.* **2013**, *15*, 358–366.

[59] O. Kahn, *Chem. Phys. Lett.* **1997**, *265*, 109–114.

[60] D. Doehnert, J. Koutecky, *J. Am. Chem. Soc.* **1980**, *102*, 1789–1796.

[61] M. Head-Gordon, *Chem. Phys. Lett.* **2003**, *372*, 508–511.

[62] D. Geuenich, K. Hess, F. Köhler, R. Herges, *Chem. Rev.* **2005**, *105*, 3758–3772.

[63] Z. Chen, C. S. Wannere, C. Corminboeuf, R. Puchta, P. von R. Schleyer, *Chem. Rev.* **2005**, *105*, 3842–3888.

22504 www.angewandte.org

© 2021 Wiley-VCH GmbH

Angew. Chem. Int. Ed. **2021**, *60*, 22496–22504